Desalination and Water Treatment
www.deswater.com

doi: 10.5004/dwt.2017.20907

86 (2017) 165–173
August

Zeolitic imidazolate framework supported on silica for removal of bromophenol blue

Shiereen Amiri, Saeedeh Hashemian*, Razeih Mohebat

Department of Chemistry, Islamic Azad University, Yazd Branch, Yazd, Iran, Tel. +9831872572; Fax: +983537266065; emails: sa_hashemian@iauyazd.ac.ir (S. Hashemian), shirinamiriazad@gmail.com (S. Amiri), raziehmohebatazad@gmail.com (R. Mohebat)

Received 16 November 2016; Accepted 9 May 2017

ABSTRACT

The zeolitic imidazolate framework (ZIF-9) and ZIF-9@SiO_2 composite were prepared and characterized by Fourier transform infrared (FTIR), scanning electron microscopy (SEM), transmission electron microscopy (TEM) and X-ray diffraction (XRD). Results of FTIR and XRD confirmed the formation of ZIF-9 and ZIF-9@SiO_2. The morphology of ZIF-9@SiO_2 was examined by SEM. TEM results showed particle size of 20 nm for ZIF-9@SiO_2. The adsorptive properties of bromophenol blue (BPB) based on ZIFs were studied. Adsorption of BPB onto ZIFs was fitted well by pseudo-second-order kinetic model. The adsorption process was followed by Langmuir isotherm model. The maximum adsorption capacity was found to be 122 mg g^{-1} at contact time 30 min and pH 3. Adsorption thermodynamics of the BPB adsorption to ZIF-9@SiO_2 was studied and the results showed that the process is spontaneous.

Keywords: Adsorption; Bromophenol blue; Composite; ZIF-9; ZIF-9@SiO_2; Zeolitic imidazolate framework

1. Introduction

Synthetic dyes originate from a number of industries, such as the textile industry, metal plating, packaging, paper industry, leather industry, cosmetics, food industry, pharmaceutical industry, tannery, Kraft bleaching, hair coloring, and rubber and plastics [1–4]. Among these various parts, the textile industry ranks first in terms of usage of dyes for coloration of fiber [5,6]. Some of the dyes are toxic and carcinogenic and have harmful effects on living organisms within short exposure periods. Thus, uses of dye contaminated water without any treatment may cause adverse effect on human health, domestic animals, wildlife and the environment. So it is necessary to treat or remove dyes from the industrial effluent before discharge [7]. Therefore, dye removal from effluent is one of the most difficult requirements challenged by dye-producing industries.

Various physical, chemical and biological treatment methods such as chemical coagulation, ozonation, membrane filtration, electrolysis, oxidation, electrochemical and biodegradation have been used for the removal of dyes from water and wastewater [8–14].

Adsorption process has been demonstrated as a potential technique for the removal of dyes from wastewater. The adsorption process was found to be the most effective and non-destructive technique and is still one of the best-known techniques that is widely used for removal of dyes from aqueous solutions [15]. Dye adsorption is a process of transfer of dye molecules from bulk solution phase to the surface of the adsorbent. It is very important to find an efficient and economic adsorbent to treat wastewater that is polluted by dyes [16]. Activated carbon is widely used as an adsorbent owing to its high dye uptake, large surface area and microporous structure [17]. However, the production of activated carbon is complex and expensive, making this technology economically non-efficient. The adsorption characteristics of dyes on various adsorbents have been extensively investigated for many purposes involving separation and purification. The different adsorbents have high affinity towards organic compounds [18–20]. Low cost, simple preparation and high adsorption capacity are a few of many added values desired for the adsorbents.

* Corresponding author.

Bromophenols are hazardous dyes and most commonly used for the dyeing of cotton, silk, paper, leather and also in manufacturing of paints and printing inks. Different sorbents were used for removal of bromophenol dyes from aqueous solutions [21–25].

Zeolitic imidazolate frameworks (ZIFs) are a new class of porous crystals with extended three-dimensional structures constructed from tetrahedral metal ions (e.g., Zn and Co) bridged by imidazolate (Im) [26]. ZIFs have attracted considerable interest in recent years because of their potential applications in adsorption/separation [27] and as a heterogeneous catalyst [28,29]. ZIFs have been broadly studied and proven to be promising materials in hydrogen storage and CO_2 capture, drug delivery, photoluminescence, sensors, solar cells, batteries, etc [30–34]. A number of these ZIFs are also used for the environmental applications to degrade organic pollutants or to reduce toxic metallic pollutants [35–40].

Recently ZIF-8, a zeolitic metal–organic framework was used as high-rate supersonic spray coating to deposit thin films [41].

The aim of this work is synthesis and characterization of (ZIF-9) and ZIF-9@SiO_2 for removal of bromophenol dye from aqueous solution.

2. Experimental

2.1. Material and methods

All chemicals were analytical grade reagents and were purchased from Merck. All of the compounds were used as received, without any further purification. Distilled water was used in all of the experiments. Bromophenol blue (BPB) as a pollutant model was used.

Fourier transform infrared (FTIR) spectra were obtained on a Bruker Tensor 27 instrument with the sample dispersed on a potassium bromide pellet. Nitrogen adsorption measurements were conducted using a Quantachrome 2200e system. The powder X-ray diffraction studies were made on Siemens, D5000 X-ray diffractometer by using Cu-K_α radiation of wave length 1.54060 Å. Elemental analysis was performed on a Rigaku RIX-3000 wavelength dispersive X-ray. Scanning electron microscopy (SEM) was performed using a Philips SEM model XL30 electron microscope. TEM images were obtained by Zeiss (S 3000) EM10C, 80 KV.

2.2. Zeolitic imidazolate framework preparation

First ZIF-9 was prepared as described previously by Zakzeski et al. [33]. 8 mmol cobalt (II) nitrate hexahydrate (2.30 g) and 64.4 mmol of methyl imidazole (5.2 mL) were dissolved separately in about 9 mL dimethylformamide (DMF). The solutions were mixed and then stirred for ~8 h, and vigorously centrifuged at 3,000 rpm, and washed thoroughly with methanol. This washing procedure was repeated three times. The purple cubic crystals were separated from the mother liquid, washed thrice with 3 mL DMF, and allowed to dry in air. The resultant crystals were dried overnight at 100°C. ZIF-9@SiO_2 composite was prepared as the same procedure. SiO_2 was calcinated to 700°C. The activated SiO_2 was cooled to room temperature. The ZIF-9 and SiO_2 (ratio 1:10 W/W) were dispersed in water and then reflexed at 70°C for 3 h. Then filtered the supernatant and washed three times with water. The ZIF-9@SiO_2 composite was dried overnight at 100°C.

2.3. Adsorption studies

BPB (4,4′-(1,1-dioxido-3*H*-2,1-benzoxathiole-3,3-diyl) bis (2,6-dibromophenol) CAS number 115–39–9 with chemical formula of $C_{19}H_{10}Br_4O_5S$ (BPB) as a sample pollutant was purchased from Merck (Germany). It has molecular weight of 669.96 g mol^{-1} (Fig. 1). A stock solution of BPB 100 mg L^{-1} in double distillated water was prepared. It was diluted subsequently whenever necessary. In order to study the effect of different parameters like the contact time, pH and sorbent dosage on the sorption capacity of BPB, various experiments have been carried out by agitation of known amount of sorbents (0.15 g) in 30 mL of BPB solution with an initial concentration 20 mg L^{-1} on rotary shaker at a constant speed of 150 rpm at room temperature (25°C). The experiment was conducted at different pH value ranging from 2 to 12. The pH was adjusted by adding a few drops of diluted 0.1 N NaOH or 0.1 N HCl and was measured by using a pH meter (Horiba, Japan). Samples were withdrawn at appropriate time intervals and centrifuged at 1,000 rpm for 10 min. UV–Vis spectrophotometer 160A Shimadzu was used for determination of concentration of BPB.

The percentage removal of BPB by the hereby adsorbent is given by:

$$\%\ \text{Removal}_{(\text{BPB})} = (C_0 - C_e)/C_0 \times 100 \quad (1)$$

where C_0 and C_e are the initial and equilibrium concentration (mg L^{-1}) of BPB, respectively. The amount of BPB adsorbed (q_e) was determined by using the following equation:

$$q_e = (C_0 - C_e)\, V/m \quad (2)$$

where V is the volume of the solutions (mL) and m is the amount (mg) of adsorbent.

Each experiment was repeated five times, and the average results were given. Relative standard deviation (%RSD)

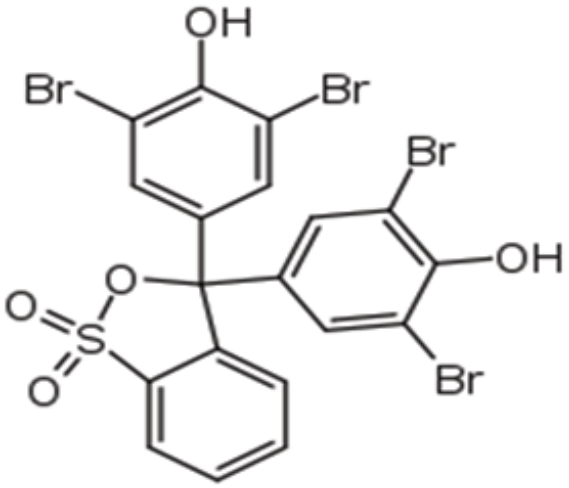

Fig. 1. Chemical structure of BPB.

was determined between 2.64%–3.1% for each points at all the experiments:

$$\% \text{ RSD} = (\Sigma (q_e - q_c)^2/n)^{1/2} \quad (3)$$

3. Results and discussion

3.1. Characterization of zeolitic imidazolate framework

The FTIR of ZIF-9, ZIF-9@SiO_2 is shown in Fig. 2. The C–H stretch vibration occurs about 3,100–3,130 cm^{-1}. The C=C stretch band of aromatic ring is around 1,600~1,500 cm^{-1}. The stretch band of N–H group observed at 3,500~2,500 cm^{-1}, which is accompanied by bend vibration of N–H group near 1,650~1,530 cm^{-1}(Fig. 2(a)). The stretch band of Co–N was observed at about 622 cm^{-1}. Fig. 2(b) shows the FTIR ZIF-9@SiO_2. The broad band from 3,400 cm^{-1} was assigned to the O–H···N hydrogen bond. This absorption band was not seen in the spectra of the ZIF-9, confirming that the 2-methylimidazole linker was fully deprotonated during the formation of the ZIF-9@SiO_2. The band 2,133 cm^{-1} is assigned to Si–H. The broad bond Si–O–Si was observed at about 1,200–1,100 cm^{-1} [42]. The IR band at 795 cm^{-1} can be assigned to Si–O–Si symmetric stretching vibrations, whereas the IR band at 457 cm^{-1} is due to O–Si–O bending vibrations (Fig. 2(b)).

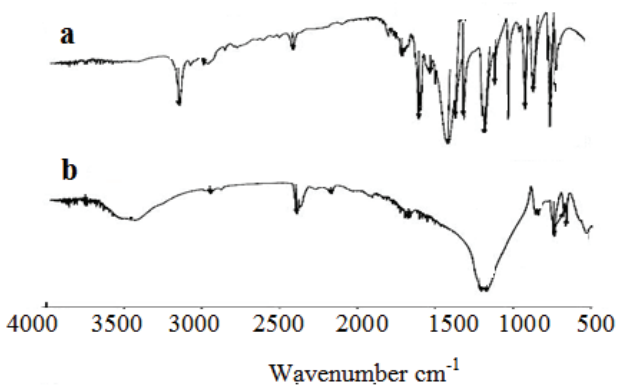

Fig. 2. FTIR spectra of (a) ZIF-9 and (b) ZIF-9@SiO_2.

The surface morphology and size of the ZIF-9 and ZIF-9@SiO_2 was examined by SEM analysis. The SEM images of ZIF-9 and ZIF-9@SiO_2 are shown in Fig. 3. The SEM image shows that the particles were at the nanoscale. The result of SEM showed that the synthesized particles of ZIF-9 were well-shaped with high-quality cubic shape crystals [43]. The ZIF-9@SiO_2 image did not have regular cubic crystals. It showed the layered and possessed a porous structure. The SEM also showed that the ZIF-9@SiO_2 nanoparticles had layer consists of randomly oriented grains. It can be observed that nanocrystals of ZIF-9 which appear brighter are supported on the darker surface of the SiO_2. It was aggregated with many nanoparticles, which resulted in a rough surface and porous structure. TEM image of ZIF-9@SiO_2 is shown in Fig. 4. It shows the particle size of 20 nm for ZIF-9@SiO_2.

The composition of the prepared ZIF-9 and ZIF-9@SiO_2 was analyzed by means of energy dispersive X-ray analysis (EDX) as shown in Table 1. The formation of ZIF-9@SiO_2 was confirmed by EDX analysis (more than 17% of Si).

The crystal phase of the ZIF-9 and ZIF-9@SiO_2 was identified by X-ray diffraction (XRD). ZIF-9 patterns show broad pattern around 2θ = 7.2°. It agrees well with patterns simulated from single crystal structure in the Cambridge Structural Database (hexagonal a = 4.920, b = 4.915, c = 5.402, alpha and beta = 90.000 and gamma = 120.000, Primitive – P3221 (154) – 3 – 113.056 – I/I_c) [44]. Fig. 5 shows the XRD patterns of ZIF-9 and ZIF-9@SiO_2.The XRD pattern was matched with the XRD pattern from Liao et al., [32] indicating that the ZIF were synthesized successfully. The diffraction at 2θ = 24.2° (100) and 31° (101) confirmed the presence of SiO_2 on

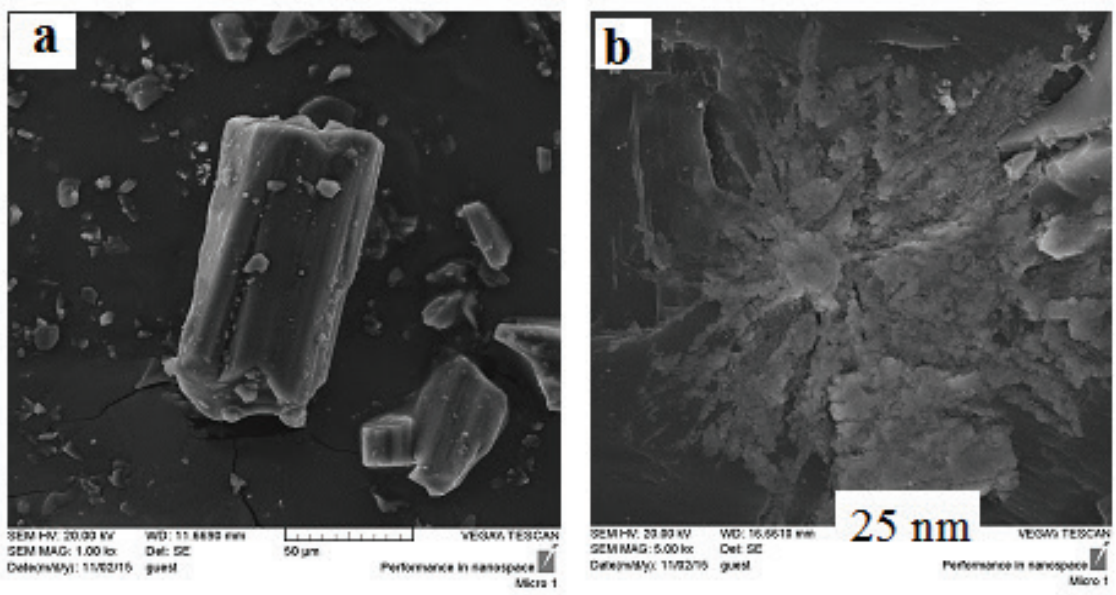

Fig. 3. SEM images of (a) ZIF-9 and (b) ZIF-9@SiO_2.

the ZIF-9@SiO_2 (Fig. 5(b)). The calculated size of the ZIF-9@SiO_2 using the Scherrer equation was in the range 18–25 nm.

The specific surface area (BET method) of the ZIF-9 and ZIF-9@SiO_2 was determined. The surface physical parameters obtained from the N_2 adsorption isotherms were shown that both the BET surface area and the total pore volume increased for ZIF-9@SiO_2. According to the obtained data, the surface areas are approximately 345 and 385 $m^2\ g^{-1}$ for the ZIF-9 and ZIF-9@Zeolite, respectively. The ZIF-9@SiO_2 showed characteristic IV type isotherms and H1 type hysteresis loops at high relative pressures.

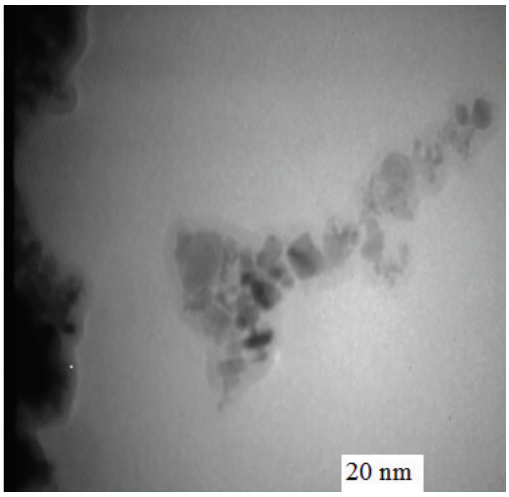

Fig. 4. TEM image of ZIF-9@SiO_2.

Table 1
Composition of elements in ZIF-9 and ZIF-9@SiO_2 by EDX

	Element %				
	Elements			Impurities	
	Co	O	C	N	Si
ZIF-9	5.3	19.8	33.79	41.09	–
ZIF-9@SiO_2	15.1	44.24	13.12	9.13	17.26

3.2. Adsorption study

The effect of varying parameters that effect on the adsorption of BPB from an aqueous solution was investigated to optimize the adsorption process. The optimum adsorption conditions, including contact time, pH, adsorbent dosage and dye concentration, were investigated in this work.

3.2.1. Effect of contact time

The effect of contact time on removal of BPB was studied, and the result is shown in Fig. 6. Large amounts of BPB were removed in the first 30 min (~90%) and reached equilibrium gradually for ZIF-9@SiO_2. After the equilibrium, adsorption efficiency was not increased significantly. So, 30 min was used as the optimal contact time. The adsorption of BPB by ZIF-9 was slower than ZIF-9@SiO_2 (equilibrium time 60 min and about 60% removal). Results also indicate that the rapid adsorption of BPB dye was observed, and then, it becomes slower near the equilibrium. It would be for that a large number of vacant surface sites are available for adsorption during the initial stage of the treatment time, and after a lapse of time, the remaining vacant surface sites are difficult to be occupied due to repulsive forces between BPB adsorbed on the surface of sorbent and solution phase.

3.2.2. Effect of initial solution pH

The effect of solution pH on removal of BPB by ZIF-9 and ZIF-9@SiO_2 was studied. pHs 2–12 were adjusted by diluted solutions of hydrochloric acid and sodium hydroxide. The results are presented in Fig. 7. In Fig. 7, the maximum BPB removal yield was observed for an initial pH around 3. As the pH value is low, the negatively charged sites on ZIF-9@SiO_2 are more protonated, hence, they are more available to adsorb BPB through the electrostatic attraction. Thus, high adsorption capacity of BPB on adsorbent occurs. It can be

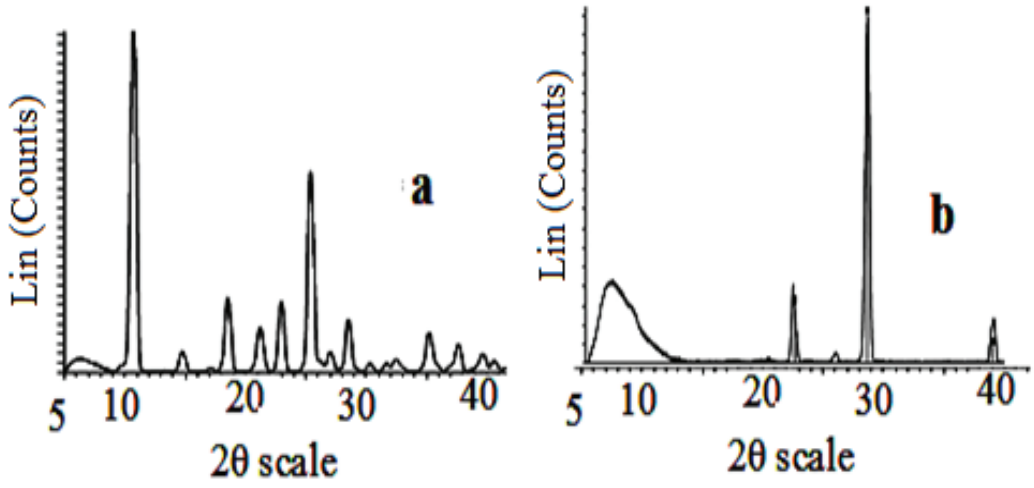

Fig. 5. XRD patterns of (a) ZIF-9 and (b) ZIF-9@SiO_2.

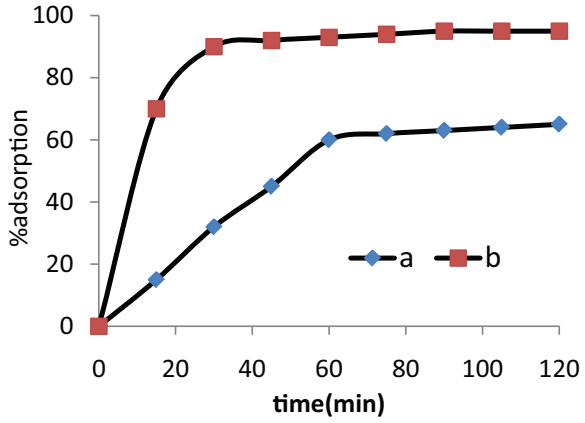

Fig. 6. Effect of the contact time on the adsorption of BPB by (a) ZIF-9 and (b) ZIF-9@SiO_2 (30 mL of BPB 20 mg L^{-1} and 0.15 g sorbents).

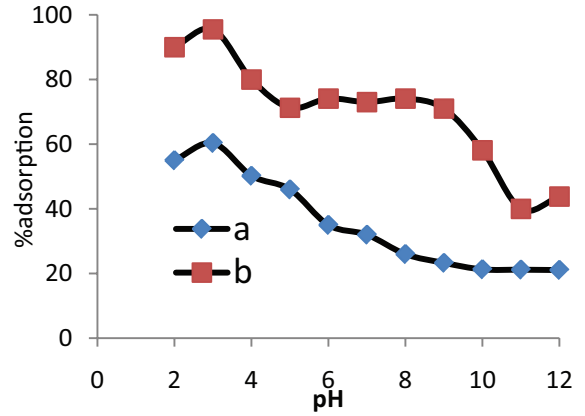

Fig. 7. Effect of pH on the adsorption of BPB by (a) ZIF-9 and (b) ZIF-9@SiO_2 (30 mL of BPB 20 mg L^{-1} and 0.15 g sorbents).

observed that the adsorption capacity of the sorbents decrease with an increase in pH of the initial solution from 3 to 6, and then reach slowly constant as the pH becomes more basic. The adsorption is highly dependent on pH of the solution, which can be interpreted in terms of electronegative property of sorbent surface. In alkaline pHs, the repulsion of negative charges on the adsorbent and BPB will reduce the adsorption of BPB. The decrease of BPB adsorption under alkaline pH condition may be due to the presence of excess OH^- ions. A negative charged surface site on the sorbent does not favor the adsorption of BPB dye due to electrostatic repulsion and causing an evident decrease in the BPB adsorption.

3.2.3. Effect of adsorbent mass

The effect of sorbent dosage on the adsorption process was studied, and the results are illustrated in Fig. 8. It is clear that the percentage of BPB removal from the aqueous solution increased from 21% to 60% for 0.01–0.3 g of ZIF-9 and from 63% to 95% for 0.01–0.15 g ZIF-9@SiO_2, respectively. The increase in the percentage of BPB removal from the aqueous solution is generally due to the greater number of active

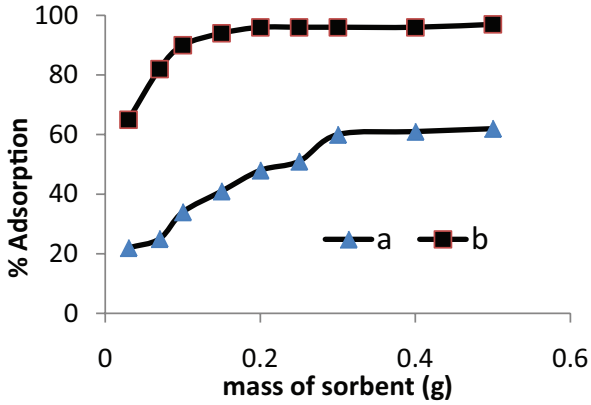

Fig. 8. Effect of sorbent mass on the adsorption of BPB by (a) ZIF-9 and (b) ZIF-9@SiO_2 (30 mL of BPB 20 mg L^{-1} and pH 3).

sites available for adsorption as a result of the increased amount of sorbent present.

When the adsorbent dosage is 0.15 g, the removal efficiency reach to steady state, where the percentage of BPB removal efficiency approached equilibrium with the value of 96%. For higher mass of sorbent, the incremental of dye removal is very small and come to equilibrium [6,7]. Therefore, positive correlation between adsorbent dose and removal efficiency is related to increasing surface area of available exchangeable sites consequently of 0.15 g dosage were selected as the optimum value.

3.2.4. Effect of initial BPB concentration

Effect of the concentration of BPB was investigated by repeating experiments with different initial concentrations (5–50 mg L^{-1}) of BPB. It is clear that the adsorption process is highly dependent on initial concentration of solution. When the initial BPB concentration varied from 5 to 50 mg L^{-1}, the adsorption capacity increased from 70% to 96% for ZIF-9@SiO_2 and from 26% to 56% for ZIF-9, respectively. The increase in adsorption of BPB with increasing initial concentration of BPB is attributed to the increase in the mass transfer driving force in high dye concentration.

3.2.5. Effect of chloride and sulfate ions on adsorption of BPB

Chloride and sulfate are common coexisting anions together with dyes in waste water. The effect of chloride and sulfate on BPB removal by ZIF-9@SiO_2 was investigated. For experiments, 30 mL of BPB 20 mg L^{-1} at pH 3 was used and 0.15 g of adsorbent was added.

It was observed that there is a small effect on BPB removal for ZIF-9@SiO_2 composite in the presence of chloride at the concentration range of 0–0.3 mol L^{-1}. The effect of SO_4^{2-} on the removal of BPB was significant at the concentration range of 0–0.2 mol L^{-1}. The removal of BPB dropped from 96% to 75% at a concentration of 0.1 mol L^{-1} SO_4^{2-}. The effect of SO_4^{2-}on BPB adsorption onto ZIF-9@SiO_2 could be attributed to competition with BPB for active sites on the adsorbent surface (the $-SO_3^{2-}$ in BPB was the active group related to adsorption). The structure of SO_4^{2-} is similar to that the $-SO_3^-$ in BPB, therefore, it is reasonable that SO_4^{2-} may complex with active sites on the composite, which leads to the decreased adsorption of BPB.

3.3. Kinetics of adsorption

3.3.1. Adsorption kinetics

To investigate the adsorption kinetics of BPB onto ZIF-9 and ZIF-9@SiO_2, pseudo-first-order and pseudo-second-order kinetic models have been applied. The linear equation for the pseudo-first-order of the kinetic model is expressed as [45]:

$$\ln q_t = \ln q_e - k_1 t \quad (4)$$

where k_1 (min^{-1}) is the rate constant of the pseudo-first order of adsorption. q_e and q_t (mg g^{-1}) are the adsorption capacities at equilibrium and at time t (min), respectively. The rate constants k_1, q_e and correlation coefficients R^2 were calculated using the slope and intercept of plots of $\ln q_e$ vs. t (Fig. 7).

The pseudo-second-order model as developed by Ho and McKay [46] has the following form:

$$t/q_t = t/q_e + 1/(k_2 q_e^2) \quad (5)$$

where q_e and q_t (mg g^{-1}) are the adsorption capacities at equilibrium and time t, k_2 (g mg^{-1} min^{-1}) is the rate constant of the pseudo-second-order adsorption. The k_2, q_e and correlation coefficient R^2 were calculated from the linear plots of t/q_t vs. t (Fig. 9).

The kinetic model with a higher correlation coefficient R^2 was selected as the most suitable one (Table 2). The results showed that adsorption kinetics of BPB onto ZIF-9 and ZIF-9@SiO_2 was fitted well by pseudo-second-order kinetic model (Figs. 9 and 10).

3.4. Adsorption isotherm

Langmuir and Freundlich adsorption isotherm models were used to describe experimental adsorption data. The Freundlich isotherm assumes heterogeneous surface energies, in which the energy term in the Langmuir equation varies as a function of the surface coverage. The adsorption Freundlich isotherm is described by the linear form following the equation [47]:

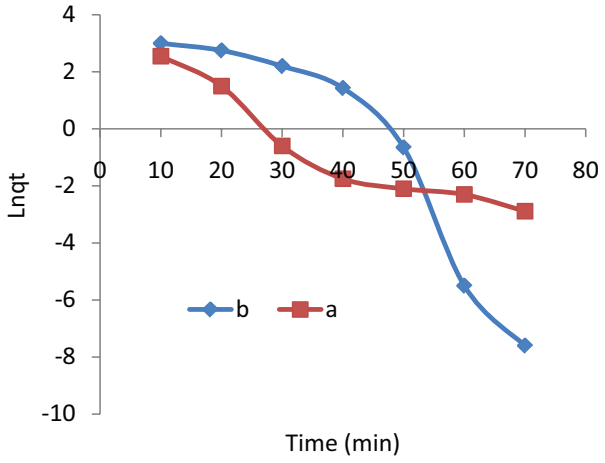

Fig. 9. Pseudo-first-order kinetics of adsorption of BPB onto (a) ZIF-9 and (b) ZIF-9@SiO_2.

$$\ln q_e = \ln K_F + (1/n) \ln C_e \quad (6)$$

where K_F and n are the Freundlich constants; C_e is the equilibrium BPB concentration in solution (mg L^{-1}). According to Eq. (6), the values of K_F and n can be determined experimentally by plotting $\ln q_e$ vs. $\ln C_e$ (Table 3).

Langmuir isotherm can be arranged in its linear form as following [48]:

$$C_e/q_e = 1/(q_{max} K_L) + C_e/q_{max} \quad (7)$$

where q_e is the amount of adsorbed BPB in the adsorbent (mg g^{-1}), C_e is the equilibrium ion concentration in solution (mg L^{-1}), K_L (L mg^{-1}) is the equilibrium constant related to the adsorption energy and q_{max} is the maximum adsorption capacity (mg g^{-1}). A linear plot is obtained when C_e/q_e is plotted against C_e (Table 3).

The high value of the regression correlation coefficient of Langmuir adsorption isotherm ($R^2 \geq 0.9$) was obtained,

Table 2
Kinetic parameters for adsorption of BPB onto ZIF-9 and ZIF-9@SiO_2

Sorbents	First order		Second order	
	R^2	k_1 (min^{-1})	R^2	k_2 (g $mg^{-1}min^{-1}$)
ZIF-9@SiO_2	0.86	1.83×10^{-1}	0.988	1.38×10^{-1}
ZIF-9	0.89	9.09×10^{-2}	0.99	8.134×10^{-3}

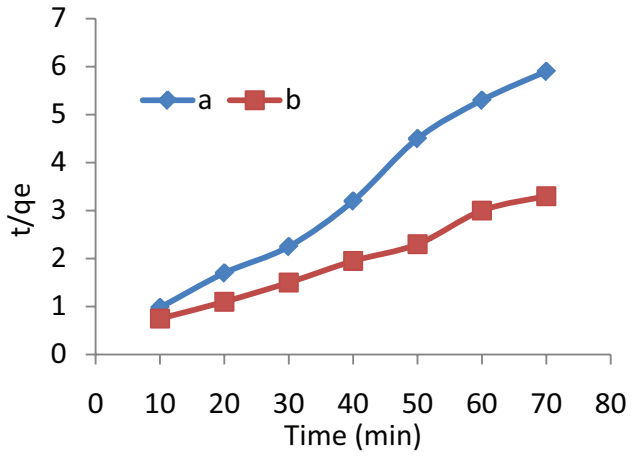

Fig. 10. Pseudo-second-order kinetics of adsorption of BPB onto (a) ZIF-9@SiO_2 and (b) ZIF-9.

Table 3
Langmuir and Freundlich constants for the adsorption of BPB onto ZIF-9 and ZIF-9@SiO_2

Freundlich				Langmuir		
Sorbent	K_F (mg g^{-1})	n	R^2	q_m (mg g^{-1})	K_L (L mg^{-1})	R^2
ZIF-9	17.5	0.49	0.75	65	0.08	0.96
ZIF-9@SiO_2	28.2	0.65	0.81	122	0.114	0.98

which indicated the adsorption of BPB onto ZIFs followed by Langmuir adsorption isotherm [49].

3.5. Thermodynamic studies

For the thermodynamic study of adsorption process, determination of the main three parameters is required. These parameters included: the standard enthalpy ($\Delta H°$), the standard free energy ($\Delta G°$) and the standard entropy ($\Delta S°$). The amounts of $\Delta H°$ and $\Delta S°$ calculated from the intercept and slope of vant Hoff plots of $\ln K_C$ vs. $1/T$, respectively:

$$\Delta G° = -RT \ln K_C \quad (8)$$

$$\ln K_C = -\Delta G°/RT = -\Delta H°/RT + \Delta S°/R \quad (9)$$

$$K_C = q_e/C_e \quad (10)$$

where K_C (L g^{-1}) is the distribution coefficient, q_e and C_e are the amount of BPB adsorbed at equilibrium (mg g^{-1}) and equilibrium concentration in solution (mg L^{-1}), respectively. R is the universal gas constant (8.314 J mol^{-1} K^{-1}), $\Delta G°$ is the standard free energy change, T is the absolute temperature and K_C is the equilibrium constant. The negative values of $\Delta G°$ showed that the process is spontaneous and feasible in the range of 293–393 K (Table 4).

3.6. Comparison of BPB onto ZIF-9 and ZIF-9@SiO_2 with other sorbents

The adsorption parameters for adsorption of phenol dyes by different sorbents are compared with ZIF-9 and ZIF-9@SiO_2 and are reported in Table 5. ZIFs in this study possess reasonable adsorption capacity in comparison with other sorbents.

3.7. Regeneration of the spent composites

The adsorption capacity of ZIF-9@SiO_2 for BPB after its regeneration has also been studied. The ZIF-9@SiO_2 was again saturated with BPB with the same initial concentration of 20 mg L^{-1}. The physical regeneration of ZIF-9@SiO_2 was done by heating at 50°C – 300°C. The complete regeneration temperature was at 250°C. The temperatures of higher than 250°C did not have significant effect on the regeneration efficiency of ZIF-9@SiO_2. Generally, the adsorption capacity of the ZIF-9@SiO_2 decreases as the number of regeneration cycle increases from 1 to 5. The adsorption capacity of the ZIF-9@SiO_2 for BPB did not show any significant decrease even after two regenerations. After three cycles 84% of BPB and after five cycles 55% of BPB was removed. The value of cycle corresponds to the adsorption capacity of the original composite. The ZIF-9@SiO_2 is simple to thermally regenerate.

Table 4
Thermodynamic parameters adsorption of BPB onto ZIF-9 and ZIF-9@SiO_2

Sorbent	$\Delta S°$ (J mol^{-1} K^{-1})	$\Delta H°$ (kJ mol)	$\Delta G°$ (kJ mol)	T (K)
ZIF-9	32.5	7.8	–1.72	293
			–2.37	313
			–3.02	333
			–3.67	353
			–4.32	373
ZIF-9@SiO_2	59.95	8.6	–8.96	293
			–10.16	313
			–11.36	333
			–12.56	353
			–13.76	373

Table 5
Comparison of adsorption parameters of ZIF-9 and ZIF-9@SiO_2 with sorbents for kind of phenol dyes

Sorbent	Kinetic	Isotherm	q_{max}	Ref
Granite	Pseudo-first-order	Freundlich	–	[20]
Activated carbon	Pseudo-second-order	Langmuir	39.68	[50]
Bentonite carbon composite	Pseudo-second-order	Freundlich	–	[51]
Supported ionic liquids	Pseudo-second-order	Langmuir	204	[52]
α-Chitin	Pseudo-second-order	Langmuir	24.390	[24]
Cola nut shell based activated carbon	Pseudo-second-order	Langmuir	6.22	[53]
Mild Steel	–	Langmuir	–	[54]
Alumina	Pseudo-second-order	Langmuir	62.897	[55]
Luffa cylindrica fibers	Pseudo-second-order	Langmuir		[56]
Sewage sludge	Pseudo-second-order	Langmuir	26.16	[57]
Silica-filled ENR/PVC	Pseudo-second-order	Freundlich, Langmuir	2.67	[58]
Lignocellulose	Pseudo-second-order	Langmuir	1.454–3.312	[59]
Mesoporous hybrid gel	Pseudo-second-order	Freundlich	–	[60]
ZIF-9	Pseudo-second-order	Langmuir	65	In this study
ZIF-9@SiO_2	Pseudo-second-order	Langmuir	122	In this study

The good regeneration results and relatively low regeneration temperature proved that the ZIF-9@SiO_2 could offer high adsorptive activity.

4. Conclusions

ZIF-9 and ZIF-9@SiO_2 were successfully prepared and characterized. The removal of BPB from aqueous solution by ZIF-9 and ZIF-9@SiO_2 was studied. The effect of varying parameters that affect the removal/adsorption process such as contact time, BPB concentration, sorbent mass and pH of solution were investigated. The adsorption of BPB on ZIFs was followed by pseudo-second-order kinetic model. The equilibrium sorption isotherm data were denoted by the Langmuir isotherm equation and maximum adsorption capacity of 65 and 122 mg g^{-1} for by ZIF-9 and ZIF-9@SiO_2, respectively.

Acknowledgment

The authors would like to gratefully acknowledge the financial support from the Research Council of Islamic Azad University of Yazd.

References

[1] S. Hashemian, A. Dehghanpor, M. Moghahed, $Cu_{0.5}Mn_{0.5}Fe_2O_4$ nanospinels as potential sorbent for adsorption of brilliant green, J. Ind. Eng. Chem., 24 (2015) 308–314.
[2] G. Crini, Non-conventional low-cost adsorbents for dye removal: a review, Bioresour. Technol., 97 (2006) 1061–1085.
[3] N.A. Abdullah, R. Othaman, I. Abdullah, N. Jon, A. Baharum, Studies on the adsorption of phenol red dye using silica-filled ENR/PVC Beads, J. Emerg. Trends Eng. Appl. Sci., 3 (2012) 845–850.
[4] S. Hashemian, M. Salimi, Nano composite a potential low cost adsorbent for removal of cyanine, Chem. Eng. J., 188 (2012) 57–63.
[5] U. Singh, R. Kumar Kaushal, Treatment of wastewater with low cost adsorbent – a review, 3 (2013) 33–42.
[6] S. Hashemian, A. Foroghimoqhadam, Effect of copper doping on $CoTiO_3$ Ilmenite type nano particles for removal of congo red from aqueous solution, Chem. Eng. J., 235 (2014) 299–306.
[7] S. Hashemian, B. Sadeghi, M. Mangeli, Hydrothermal synthesis of nano cavities of Al-MCF for adsorption of indigo carmine from aqueous solution, J. Ind. Eng. Chem., 21 (2015) 423–427.
[8] E. Guibal, J. Roussy, Coagulation and flocculation of dye-containing solutions using a biopolymer (Chitosan), React. Funct. Polym., 67 (2007) 33–42.
[9] L. Szpyrkowicz, C. Juzzolino, S.N. Kaul, A comparative study on oxidation of disperse dyes by electrochemical process, ozone, hypochlorite and fenton reagent, Water Res., 35 (2001) 2129–2136.
[10] Y. Fu, T. Viraraghavan, Fungal decolorization of dye wastewaters: a review; Bioresour Technol., 79 (2001) 251–262.
[11] J. Chen, L. Zhu, Catalytic degradation of orange II by UV-Fenton with hydroxyl-Fe-pillared bentonite in water, Chemosphere, 65 (2006) 1249–1255.
[12] V.K. Gupta, R. Jain, S. Varshney, Electrochemical removal of the hazardous dye reactofix red 3 BFN from industrial effluents, J. Coll. Inter. Sci., 312 (2007) 292–296.
[13] L. Gomes, D.W. Miwa, G.R.P. Malpass, A.J. Motheo, Electrochemical degradation of the dye reactive orange 16 using electrochemical flow-cell, J. Braz. Chem. Soc., 22 (2011) 223–229.
[14] P. Chulhwan, Y. Lee, T.H. Kim, B. Lee, J. Lee, S. Kim, Decolorization of three acid dyes by enzymes from fungal strains, J. Microbiol. Biotechnol., 14 (2004) 1190–1195.
[15] S. Hashemian, Removal of Acid Red 151 from water by adsorption onto nano-composite $MnFe_2O_4$/kaolin, Main Group Chem., 10 (2011) 105–114.
[16] S. Hashemian, M. Monshizadeh, Removal of methylene blue from aqueous solution by nano $LaFeO_3$ particles, Main Group Chem., 12 (2013) 113–124.
[17] M. Hema, S. Arivoli, Adsorption kinetics and thermodynamics of malachite green dye unto acid activated low cost carbon, J. Appl. Sci. Environ. Manage., 12 (2008) 43–51.
[18] S. Hashemian, K. Salari, Z. Atashi Yazdi, Preparation of activated carbon from agricultural wastes (almond shell and orange peel) for adsorption of 2-pic from aqueous solution, J. Ind. Eng. Chem., 20 (2014) 1892–1900.
[19] S. Hashemian, J. Shayegan, A comparative study of cellulose agricultural wastes (almond shell, pistachio shell, walnut shell, tea waste and orange peel) for adsorption of violet b dye from aqueous solutions, Orient. J. Chem., 30 (2014) 2091–2098.
[20] L.H. Kadhim, Granite as an adsorption surface for the removal of bromo phenol red, bromo cresol green and leishman's stain from aqueous solutions, J. Basrah Res. Sci., 38 (2012) 106–116.
[21] F.M.S.E. El-Dars, H.M. Ibrahim, H.A.B. Farag, M. Zakaria Abdelwahhab, M.E.H. Shalabi, Adsorption kinetics of bromophenol blue and eriochrome black t using bentonite carbon composite material, Int. J. Sci. Eng. Res., 6 (2015) 679–688.
[22] A.O. Dada, A.A. Inyinbor, A.P. Oluyori, Comparative adsorption of dyes unto activated carbon prepared from maize stems and sugar cane stems, IOSR J. Appl. Chem., 2 (2012) 38–43.
[23] H. Altaher, T.E. Khalil, R. Abubeah, The effect of dye chemical structure on adsorption on activated carbon: a comparative study, Color. Technol., 130 (2014) 205–214.
[24] S. Dhananasekaran, R. Palanivel, S. Pappu, Adsorption of methylene blue, bromophenol blue and coomassie brilliant blue by α-chitin nanoparticles, J. Adv. Res., 7 (2016) 113–118.
[25] S.M.A. El Gamal, M.S. Amin, M.A. Ahmed, Removal of methyl orange and bromophenol blue dyes from aqueous solution using Sorel's cement nanoparticles, J. Environ. Chem. Eng., 3 (2015) 1702–1712.
[26] Y.R. Lee, J. Kim, W.S. Ahn, Synthesis of metal-organic frameworks: a mini review, Korean J. Chem. Eng., 30 (2013) 1667–1680.
[27] S. Bhattacharjee, M.S. Jang, H.J. Kwon, W.S. Ahn, Zeolitic imidazolate frameworks: synthesis, functionalization, and catalytic/adsorption applications, Catal. Surv. Asia, 18 (2014) 101–127.
[28] K.Y. Andrew Lin, H.A. Chang, Zeolitic imidazole framework-67(ZIF67) as a heterogeneous catalyst to activate peroxy mono sulfate for degradation of Rhodamine B in water, J. Taiwan Inst. Chem. Eng., 53 (2015) 40–45.
[29] M. Zhao, S. Ou, C.D. Wu, Porous metal–organic frameworks for heterogeneous biomimetic catalysis, Acc. Chem. Res., 47 (2014) 1199–207.
[30] D. Danaci, R. Singh, P. Xiao, P.A. Webley, Assessment of ZIF materials for CO_2 capture from high pressure natural gas streams, Chem. Eng. J., 280 (2015) 486–493.
[31] A. Phan, C.J. Doonan, F.J. Uribe-romo, C.B. Knobler, M. O'Keeffe, O. Yaghi, Synthesis, structure, and carbon dioxide capture properties of zeolitic imidazolate frameworks, Acc. Chem. Res., 43 (2010) 58–67.
[32] Y.T. Liao, S. Dutta, C.H. Chien, C.C. Hu, F.K. Shieh, C.H. Lin, K.C.W. Wu, Synthesis of mixed-ligand zeolitic imidazolate framework (ZIF-8–90) for CO_2 adsorption, J. Inorg. Organomet. Polym. Mater., 25 (2015) 251–258.
[33] J. Zakzeskia, A. Debczak, P.C.A. Bruijnincx, B.M. Weckhuysen, Catalytic oxidation of aromatic oxygenates by the heterogeneous catalyst Co-ZIF-9, Appl. Catal., A, 394 (2011) 79–85.
[34] R.V. Surendar, A.C. Moises, Metal organic framework membranes for carbon dioxide separation, Chem. Eng. Sci., 124 (2015) 3–19.
[35] H.C. Zhou, S. Kitagawa, Metal organic frameworks (MOFs), Chem. Soc. Rev., 43 (2014) 5415–5418.
[36] M. Alvaro, E. Carbonell, B. Ferrer, F.X. Llabrési Xamena, H. Garcia, Semiconductor behavior of a metal–organic framework (MOF), Chemistry, 13 (2007) 5106–5012.

[37] K.Y. Lin, H.A. Chang, Ultra-high adsorption capacity of zeolitic imidazole framework-67 (ZIF-67) for removal of malachite green from water, Chemosphere, 139 (2015) 624–631.
[38] D. Liu, Y. Wu, Q. Xia, Z. Li, Experimental and molecular simulation studies of CO_2 adsorption on zeolitic imidazolate frameworks: ZIF-8 and amine-modified ZIF-8, Adsorption, 19 (2013) 25–37.
[39] J. Li, Y. Wu, Z. Li, B. Zhang, M. Zhu, X. Hu, Y. Zhang, F. Li, Zeolitic imidazolate framework-8 with high efficiency in trace arsenate adsorption and removal from water, J. Phys. Chem. C., 118 (2014) 27382–27387.
[40] J.Q. Jiang, C.X. Yang, X.P. Yan, Zeolitic imidazolate framework-8 for fast adsorption and removal of benzotriazoles from aqueous solution, ACS Appl. Mater. Interfaces, 5 (2013) 9837–9842.
[41] Q. Liu, Z.X. Low, L. Li, A. Razmjou, K. Wang, J. Yao, H. Wang, ZIF-8/Zn_2GeO_4 nanorods with an enhanced CO_2 adsorption property in an aqueous medium for photocatalytic synthesis of liquid fuel, J. Mater. Chem. A, 8 (2013) 11563–11569.
[42] L.T.L. Nguyen, K.K.A. Le, N.T.S. Phan, A zeolite imidazolate framework ZIF-8 catalyst for friedel-crafts acylation, Chin. J. Catal., 33 (2012) 688–696.
[43] M. Gustafsson, X. Zou, Crystal formation and size control of zeolitic imidazolate frameworks with mixed imidazolate linkers, J. Porous Mater., 20 (2013) 55–63.
[44] Y. Li, F. Liang, H. Bux, W. Yang, J. Caro, Zeolitic imidazolate framework ZIF-7 based molecular sieve membrane for hydrogen separation, J. Membr. Sci., 354 (2010) 48–54.
[45] S. Lagergren, About the theory of so-called adsorption of soluble substances, K. Sven. Vetensk.akad. Handl., 24 (1898) 1–39.
[46] Y.S. Ho, G. McKay, The kinetics of sorption of basic dyes from aqueous solution by sphagnum moss peat, Can. J. Chem. Eng., 76 (1998) 822–827.
[47] H.M.F. Freundlich, Over the adsorption in solution, J. Phys. Chem., 57 (1906) 385–470.
[48] I. Langmuir, The adsorption of gases on plane surfaces of glass, mica and platinum, J. Am. Chem. Soc., 40 (1918) 1361–1403.
[49] C.S. Wu, Z.H. Xiong, C. Li, J.M. Zhang, Zeolitic imidazolate metal organic framework ZIF-8 with ultra-high adsorption capacity bound tetracycline in aqueous solution, RSC Adv., 5 (2015) 82127–82137.
[50] H. Altaher, T.E. Khalil, R. Abubeah, The effect of dye chemical structure on adsorption on activated carbon: a comparative study, Color. Technol., 130 (2014) 205–214.
[51] F.M.S.E. El-Dars, H.M. Ibrahim, H.A.B. Farag, M.Z. Abdelwahhab, M.E.H. Shalabi, Adsorption kinetics of bromophenol blue and eriochrome black t using bentonite carbon composite material, Int. J. Sci. Eng. Res., 6 (2015) 679–688.
[52] J. Liu, S. Yao, L. Wang, W. Zhu, J. Xu, H. Song, Adsorption of bromophenol blue from aqueous samples by novel supported ionic liquids, J. Chem. Technol. Biotechnol., 89 (2014) 230–238.
[53] R.B. Lekene Ngouateu, P.M.A. Kouoh Sone, J. Ndi Nsami, D. Kouotou, P.D. Belibi Belibi, J. Ketcha Mbadcam, Kinetics and equilibrium studies of the adsorption of phenol and methylene blue onto cola nut shell based activated carbon, Int. J. Curr. Res. Rev., 7 (2015) 1–9.
[54] A.I. Onen, O.N. Maitera, J. Joseph, E.E. Ebenso, Corrosion inhibition potential and adsorption behaviour of bromophenol blue and thymol blue dyes on mild steel in acidic medium, Int. J. Electrochem. Sci., 6 (2011) 2884 – 2897.
[55] M.J. Iqbal, M.N. Ashiq, Thermodynamics and kinetics of adsorption of dyes from aqueous media onto alumina, J. Chem. Soc. Pak., 32 (2010) 419–428.
[56] O. Abdelwahab, N.K. Amin, Adsorption of phenol from aqueous solutions by *Luffa cylindrica* fibers: kinetics, isotherm and thermodynamic studies, Egypt. J. Aquat. Res., 39 (2013) 215–223.
[57] S. Bousbaa, A.H. Meniai, Removal of phenol from water by adsorption onto sewage sludge based adsorbent, Chem. Eng. Trans., 40 (2014) 235–240.
[58] A.N. Amni, O.R., Abdullah, I. Nazwa, J.B. Azizah, Studies on the adsorption of phenol red dye using silica-filled ENR/PVC beads, J. Emerging Trends Eng. Appl. Sci., 3 (2012) 845–850.
[59] R.M.K. Vala, L. Tichagwa, E.D. Dikio, Evaluation of N-terminated siloxanes grafted onto lignocellulose as adsorbent for the removal of phenol red from water, Int. J. Environ. Sci. Technol., 12 (2015) 2723–2730.
[60] Y. Laijiang, W. Zhijian, K. Taehoon, L. Kangtaek, Kinetics and thermodynamics of bromophenol blue adsorption by a mesoporous hybrid gel derived from tetra ethoxysilane and bis(trimethoxysilyl) hexane, J. Coll. Inter. Sci., 300 (2006) 526–535.